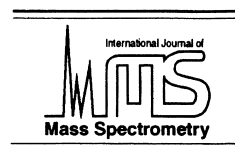




ELSEVIER

International Journal of Mass Spectrometry 204 (2001) 87–100



Large anhydrous polyaniline ions: substitution of Na^+ for H^+ destabilizes folded states

John A. Taraszka, Anne E. Counterman, David E. Clemmer*

Department of Chemistry, Indiana University, Bloomington, IN 47405, USA

Received 9 March 2000; accepted 15 July 2000

Abstract

The conformations of a series of anhydrous sodiated polyaniline ions ($[\text{Ala}_n + 3\text{Na}]^{3+}$, where $n = 18\text{--}36$) have been examined in the gas phase by ion mobility measurements and molecular modeling simulations. The experimental results indicate that these ions exist as highly extended conformations. There is no strong evidence for a folded state, observed previously for a series of analogous protonated polyanilines ($[\text{Ala}_n + 3\text{H}]^{3+}$, where $n = 24\text{--}41$) (A.E. Counterman, D.E. Clemmer, *J. Am. Chem. Soc.*, submitted). Molecular dynamics simulations for the $[\text{Ala}_n + 3\text{Na}]^{3+}$ ions also indicate that extended structures are favored. The simulations show that extensive helical regions are present; however, near the sites where Na^+ ions are attached, helical regions appear to be substantially disrupted by intramolecular charge solvation of the Na^+ . Simulations of some $[\text{Ala}_n + 3\text{Na}]^{3+}$ charge site assignments show evidence for structures that are similar to folded structures observed for analogous $[\text{Ala}_n + 3\text{H}]^{3+}$ ions; however, the calculated energy gap between the folded and unfolded states for the triply sodiated system is slightly greater than the gap in analogous protonated polyanilines. We propose this as a possible explanation for the absence of experimental evidence for a folded state in the sodiated system. (*Int J Mass Spectrom* 204 (2001) 87–100) © 2001 Elsevier Science B.V.

Keywords: Polyaniline; Ion mobility; Sodium; Stability; Electrospray

1. Introduction

Factors that influence the stability of secondary and tertiary structure in peptides and proteins have attracted significant experimental and theoretical attention [1]. Recently, several groups have examined the conformations of anhydrous protein and peptide ions in the gas phase, where structures are constrained by only intramolecular interactions [2–9]. It is believed that by comparing gas-phase and solution structures that it will be possible to distinguish char-

acteristics that are intrinsic to the polypeptide chain from those that are driven by solvent interactions [2,10].

Currently, structural measurements for several proteins [7–9], an array of peptides [6,11–16], a few saccharides [17], and nucleotide oligomers [18] in the gas phase have been reported. There is now evidence for several general structural types. Ion mobility [6,13,15,16], molecular modeling [19], and some other techniques [20] have shown that many small (~5–15 residue) singly protonated peptide sequences favor an array of largely nonspecific globular conformations, in which the charge site is solvated by interactions with electronegative groups in the

* Corresponding author. E-mail: clemmer@indiana.edu

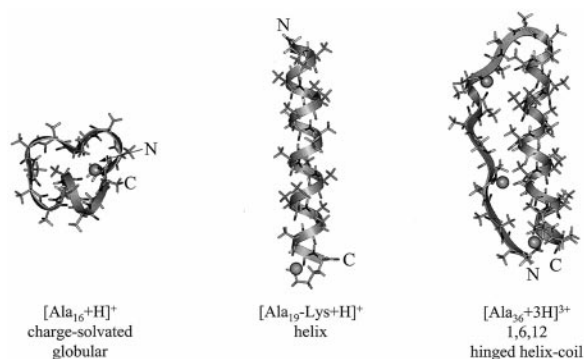


Fig. 1. Generalized structural motifs for anhydrous peptide ions: a compact globule, extended helix, and a hinged helix-coil state represented by $[\text{Ala}_{16} + \text{H}]^+$ (protonated on the N-terminal amino group), $[\text{Ala}_{19} - \text{Lys} + \text{H}]^+$ (protonated on the C-terminal lysine; [12]), and $[\text{Ala}_{36} + 3\text{H}]^{3+}$ (protonated at the $i = 1, 6,$ and 12 positions), respectively. Protonation sites are indicated as “close-packed” spheres. See text for discussion.

polypeptide. An example is shown in Fig. 1 for $[\text{Ala}_{16} + \text{H}]^+$, having a single proton attached at the basic amino terminus. Several other small singly charged homopolymers such as nonamers of polyvaline, polyisoleucine, polyileucine, polyglutamine, polythreonine, polyphenylalanine, and polytryptophan [16] as well as an array of small tryptic fragments [15] also appear to have roughly spherical shapes. A general feature of many of the molecular modeling studies of these systems is that there are many low-lying configurations which effectively solvate the charge. The observation that the charged site (and many polar groups) are situated in the interior of many peptides, whereas nonpolar groups are prevalent on the peptide surface [6,13,16] can be rationalized by considering the nonpolar nature of the vacuum environment [10]; to a first approximation many small peptides appear to adopt geometries that are effectively inside-out relative to their expected solution structures [16].

Fenselau's, Jarrold's, and our group have reported evidence for helical structures in the gas phase [5,12,23]. Fenselau's kinetic energy release data for metastable ions suggest that triply protonated mellitin, which forms helices under a variety of solution conditions, may also have helix-like character at the transition state for dissociation [5]. Based on solution studies [21] and consideration of the vacuum environ-

ment, it is expected that sequences that are rich in alanine should form helices in the gas phase. The globular state for the $[\text{Ala}_n + \text{H}]^+$ ions noted above arises because protonation at the N-terminal amino group opposes the helix dipole; the system sacrifices helical character in order to allow the electronegative carbonyl groups to solvate the charge [13]. Hudgins and Jarrold designed stable helices by blocking the N-terminal protonation site and adding a basic lysine as the C-terminal residue [12]. An example of a stable helix is shown for $[\text{Ala}_{19} - \text{Lys} + \text{H}]^+$ in Fig. 1. Here, the favorable orientation of the charged site with the direction of the helix dipole allows the charge site to be effectively capped by interactions with carbonyl groups near the end of the peptide. The ability to stabilize helices by addition of a single charged residue would seem to be extremely important; comparison of the abilities of different $[\text{Xxx}_n - \text{Lys} + \text{H}]^+$ systems (where Xxx is a naturally occurring amino acid) to form helices would allow an intrinsic helicity scale to be developed [14]. With this in mind, it has been shown that $[\text{Gly}_n - \text{Lys} + \text{H}]^+$ ($n = 5 - 19$) do not form helices—thus, the relative ordering of helix propensity $\text{Gly} < \text{Ala}$ in the gas phase is the same as in solution [22].

We have recently reported that longer triply protonated polyalanine ($n = 18 - 41$) ions can exist as extended structures that are largely helical [23]. Our molecular modeling simulations suggest that an important factor in the formation of extended helical structures is that the net position of charge (associated with the three sites) is distributed on the C-terminal side of the peptide. That is, for a peptide with n residues, extended helices are apparent when the three protons are placed at i th locations (i.e. N-H backbone groups where the N-terminus is defined as $i = 1$) such that $\sum i/3 > n/2$. It appears that elongated structures are formed in which $90 \pm 10\%$ of residues are involved in $i \rightarrow i + 4$ hydrogen bonds associated with α -helical regions.

An interesting feature of large triply protonated polyalanine peptides is that an additional state—corresponding to a more compact conformation—is observed experimentally for peptides with 24 to 41 residues [23]. Molecular modeling simulations show

that when the net distribution of the three charges is distributed on the N-terminal side of the peptide, i.e. $\sum i/3 < n/2$, a folded hinged helix-coil motif arises. An example of this motif is also shown in Fig. 1 for the $[\text{Ala}_{36} + 3\text{H}]^{3+}$ peptide where protons were attached at the $i = 1, 6,$ and 12 positions. A general feature of this type of structure is that upon folding, the interaction of the N-terminal protonation site with the C-terminal portion of the peptide stabilizes a helical region (Fig. 1). This type of motif appears for all sizes that we have modeled and calculated collision cross sections for model states are in agreement with experiment [24]. The substantial deviation in behavior of this state from the random globules and well-defined helical states has led us to propose it as a third general motif (Fig. 1) [23]. The hinged helix coil is particularly interesting because the first fold appears to compete directly with the helix conformation.

In this article we present an initial report of ion mobility experiments for a series of sodiated polyalanines $[\text{Ala}_n + 3\text{Na}]^{3+}$ ($n = 18\text{--}36$). Molecular dynamics simulations show that the sodiated peptides also form extended structures with large helical regions—similar to the helices observed for $[\text{Ala}_{18} + 3\text{H}]^{3+}$ to $[\text{Ala}_{39} + 3\text{H}]^{3+}$. The simulations suggest that a folded helix-coil state can form if the net charge associated with the positions of Na^+ ions is located on the N-terminal portion of the peptide. However, this state appears to be relatively high in energy. We find no experimental evidence for the hinged helix-coil state. The combined experimental and theoretical results suggest that solvation of the substantially larger Na^+ ions destabilizes the folded motif. It is also possible that the dearth of folded structures arises from differences that arise during the formation of the sodiated and protonated ions.

2. Experimental

2.1. General

Ion mobility techniques and their application to biomolecular ions have been discussed in detail pre-

viously [25,26]. The high-pressure high-resolution ion mobility/time-of-flight instrument used here has also been described previously [27,28]. Protonated polyalanine peptides were generated by electrospraying a 0.5 mg mL^{-1} solution (49:49:2 water:acetonitrile:acetic acid) of mixtures of polyalanines (Sigma, 1000–5000 MW). Sodiated polyalanine species are generated by electrospraying a 0.5 mg mL^{-1} solution (50:50 water:acetonitrile) of mixtures of polyalanines with 5 mM of sodium acetate. Ion mobility and mass spectrometric measurements were performed using a nested drift (flight) time acquisition scheme [27]. In these experiments a $300 \mu\text{s}$ pulse of ions is introduced into the drift region using a fine wire mesh ion gate. The drift region is operated at a pressure of ~ 150 Torr and an electric field strength of 137.4 V cm^{-1} . Under these conditions, drift velocities are small when compared with the thermal velocity of the helium buffer gas; drift time distributions reflect an average of all possible orientations of all the conformations that are present. Flight times were measured using a reflectron geometry time-of-flight mass spectrometer and are significantly shorter than the drift times, allowing data for all components of the ion mixture to be accumulated simultaneously, as described previously [27]. We refer to this approach as a nested drift (flight) time measurement.

2.2. Cross sections and effective asphericity scale

Experimental drift times are converted to cross sections using [26]

$$\Omega = \frac{(18\pi)^{1/2}}{16} \frac{ze}{(k_b T)^{1/2}} \left(\frac{1}{m_I} + \frac{1}{m_{\text{He}}} \right)^{1/2} \frac{760ET}{273.2LPN} t_D \quad (1)$$

where t_D is the drift time, E is the electric field strength in the drift tube, L is the length of the drift tube, P is the buffer gas pressure, z is the charge state, N is the neutral number density, T is the drift tube temperature, k_b is Boltzmann's constant, e is the charge of an electron, and m_I and m_{He} are the masses of polyalanine and helium, respectively. In addition, it is necessary to correct for the flight times of ions in other parts of the instrument as well as the ions'

energies at the exit of the drift tube in the presence and absence of buffer gas. This correction is small (~ 150 – $250 \mu\text{s}$) in these experiments.

Differences in collision cross sections between globular and helical conformations decrease with decreasing size. In order to compare helical and globular conformations over a wide range of sizes it is useful to define an effective asphericity scale (Ω_{asp}) given by

$$\Omega_{\text{asp}} = \frac{\Omega - \Omega_{\text{sphere}}}{\Omega_{\text{linear}} - \Omega_{\text{sphere}}} \quad (2)$$

where Ω is the experimental or calculated cross section; $\Omega_{\text{sphere}} = -9.49 \times 10^{-4} n^3 + -0.213n^2 + 16.2n + 38.1$, as determined from a fit to experimental cross sections for globular $[\text{Ala}_n + \text{H}]^+$ ions where n is the number of residues [23]; and $\Omega_{\text{linear}} = 25.95n + 27.75$, as determined from a fit to calculated cross sections for linear structures (20–50 residues). On this scale, completely spherical conformations have $\Omega_{\text{asp}} \equiv 0$ and limiting linear structures generated by molecular modeling have $\Omega_{\text{asp}} \equiv 1$. The scale is referred to as an effective asphericity because it depends only on relative cross sections; that is, the effective asphericity does not account for the fact that different structures (e.g. oblate and prolate geometries) could have identical collision cross sections.

2.3. Molecular modeling and cross section calculations for trial structures

Molecular dynamics simulations were performed for $[\text{Ala}_n + 3\text{Na}]^{3+}$ ions ($n = 27, 30, 34$) using the extensible systematic force field on BIOSYM DISCOVER 3.0.0 software [29]. All simulations were performed at an effective temperature of 300 K and carried out for at least 0.25 ns. Some calculations were conducted for 1.0 ns; no large differences in the results for the different timescales were observed. During the simulations, atomic coordinates for 50 different structures were acquired in sequential 5 ps intervals. These structures were energy minimized and collision cross sections were calculated using the exact hard spheres scattering (EHSS) method [30]. The EHSS calculation

ignores potential interactions but does include a scattering term. Calculated cross sections are modified by a calibration term (determined by comparison of EHSS cross sections to a more rigorous trajectory method), as described previously [23]. All simulations described here were initiated using α -helical conformations; simulations started from other conformations (hinged helix coil or linear) yield energy minimized structures that have higher calculated energies and are generally not in agreement with the experimental results. Equation (2) is used to convert calculated cross sections for trial conformers into effective asphericities for comparison with experimental results.

3. Results and discussion

3.1. Mass spectra of protonated and sodiated polyalanines

Fig. 2 shows mass spectra for protonated and sodiated polyalanine ions formed by electrospraying solutions containing acetic acid and sodium acetate, respectively. The spectrum corresponding to the protonated peptides shows representative peaks at m/z ratios of 685.3, 717.9, 729.7, 756.3, and 765.2 (as well as many others). These m/z ratios are consistent with formation of the $[\text{Ala}_{19} + 2\text{H}]^{2+}$, $[\text{Ala}_{30} + 3\text{H}]^{3+}$, $[\text{Ala}_{10} + \text{H}]^+$, $[\text{Ala}_{21} + 2\text{H}]^{2+}$, and $[\text{Ala}_{32} + 3\text{H}]^{3+}$ ions which have calculated m/z values (isotopic averages) of 685.5, 718.0, 730.0, 756.6, and 765.4, respectively. In some cases, additional features in the data complicate assignments; here, as shown below, the simplifying nature of the mobility separation in the two-dimensional datasets allows unambiguous assignments to be made. In all, under the experimental conditions employed in these studies, we observe the $[\text{Ala}_n + \text{H}]^+$ ions for $n = 5$ – 18 , $[\text{Ala}_n + 2\text{H}]^{2+}$ for $n = 9$ – 29 , and $[\text{Ala}_n + 3\text{H}]^{3+}$ for $n = 18$ – 41 .

The mass spectrum for the sodiated peptides is substantially more complicated and not all of the less intense peaks can be assigned. Again, the initial separation associated with the two-dimensional datasets are useful in assigning the most intense peaks.

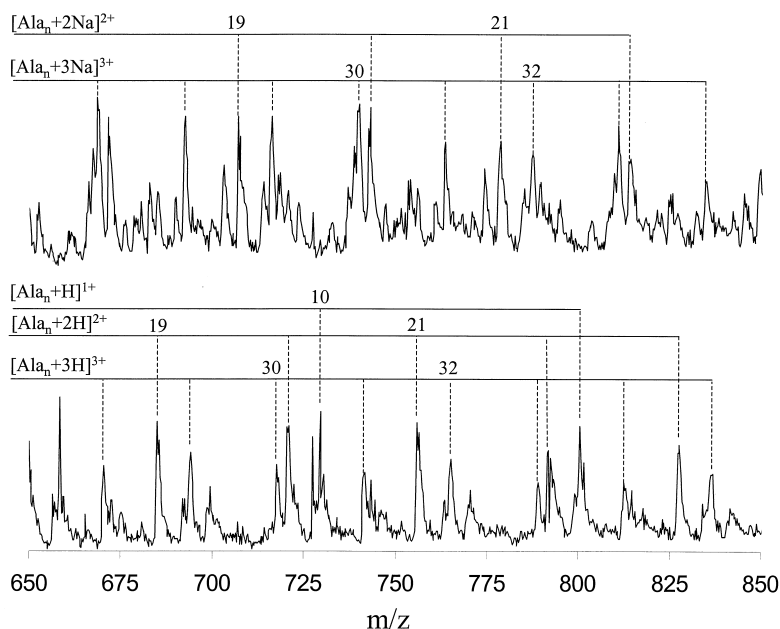


Fig. 2. Example mass spectra obtained for (a) $[\text{Ala}_n + x\text{H}]^{x+}$ ions formed by electrospraying a 0.5 mg mL^{-1} solution of polyalanines (Sigma, 1000–5000 MW) in 49:49:2 water:acetonitrile:acetic acid solvent system; and (b) $[\text{Ala}_n + x\text{Na}]^{x+}$ ions formed by electrospraying a 0.5 mg mL^{-1} solution of polyalanines in 50:50 water:acetonitrile with 5 mM sodium acetate. The numbering system associated with the solid horizontal and dashed vertical lines denotes the number of alanine residues.

Example intense peaks at $m/z = 707.1, 740.0, 778.7,$ and 787.4 correspond to the $[\text{Ala}_{19} + 2\text{Na}]^{2+},$ $[\text{Ala}_{30} + 3\text{Na}]^{3+},$ $[\text{Ala}_{21} + 2\text{Na}]^{2+},$ and $[\text{Ala}_{32} + 3\text{Na}]^{3+}$ ions (having calculated m/z values of 707.4, 740.0, 778.5, and 787.4). A majority of the relatively intense peaks can be assigned to other sizes of $[\text{Ala}_n + 2\text{Na}]^{2+}$ and $[\text{Ala}_n + 3\text{Na}]^{3+}$ ions. Peaks corresponding to $[\text{Ala}_n + \text{Na}]^+$ ions are substantially lower in intensity, and often overlap with other features in the mass spectrum; the two-dimensional mobility separation was required to assign these ions (see below). Overall, we observe features corresponding to $[\text{Ala}_n + \text{Na}]^+$ for $n = 5\text{--}10,$ $[\text{Ala}_n + 2\text{Na}]^{2+}$ for $n = 11\text{--}24,$ and $[\text{Ala}_n + 3\text{Na}]^{3+}$ for $n = 18\text{--}36.$

3.2. Nested drift (flight) time distributions for protonated and sodiated polyalanine

Fig. 3 shows two-dimensional plots of small regions of nested drift (flight) time data recorded for the protonated and sodiated polyalanine systems. Several

differences between these distributions are apparent. Maximum intensities for the family of $[\text{Ala}_n + 2\text{Na}]^{2+}$ ions are observed at longer drift times than those of corresponding sizes of $[\text{Ala}_n + 2\text{H}]^{2+}$ ions.

Examples of experimental drift time distributions, obtained by taking slices through the two-dimensional data, are shown for the $[\text{Ala}_{21} + 2\text{H}]^{2+}$ and $[\text{Ala}_{21} + 2\text{Na}]^{2+}$ ions in Fig. 4. The maximum intensity of the $[\text{Ala}_{21} + 2\text{H}]^{2+}$ peak occurs at a drift time of 23.7 ms, whereas the corresponding $[\text{Ala}_{21} + 2\text{Na}]^{2+}$ peak occurs at 26.8 ms. The 3.1 ms increase in the drift time for $[\text{Ala}_{21} + 2\text{Na}]^{2+}$ corresponds to an increase in collision cross section of $\sim 12\%.$ The differences in drift times for $[\text{Ala}_n + 2\text{Na}]^{2+}$ and $[\text{Ala}_n + 2\text{H}]^{2+}$ ions increase for larger polyalanine sizes (e.g. the 29.9 ms drift time for $[\text{Ala}_{24} + 2\text{Na}]^{2+}$ is $\sim 14\%$ greater than the 25.8 ms value measured for $[\text{Ala}_{24} + 2\text{H}]^{2+}).$ These changes in mobilities are substantially greater than effects associated with differences in the Na^+ and H^+ ion sizes. Thus, there must be substantial changes in the overall peptide

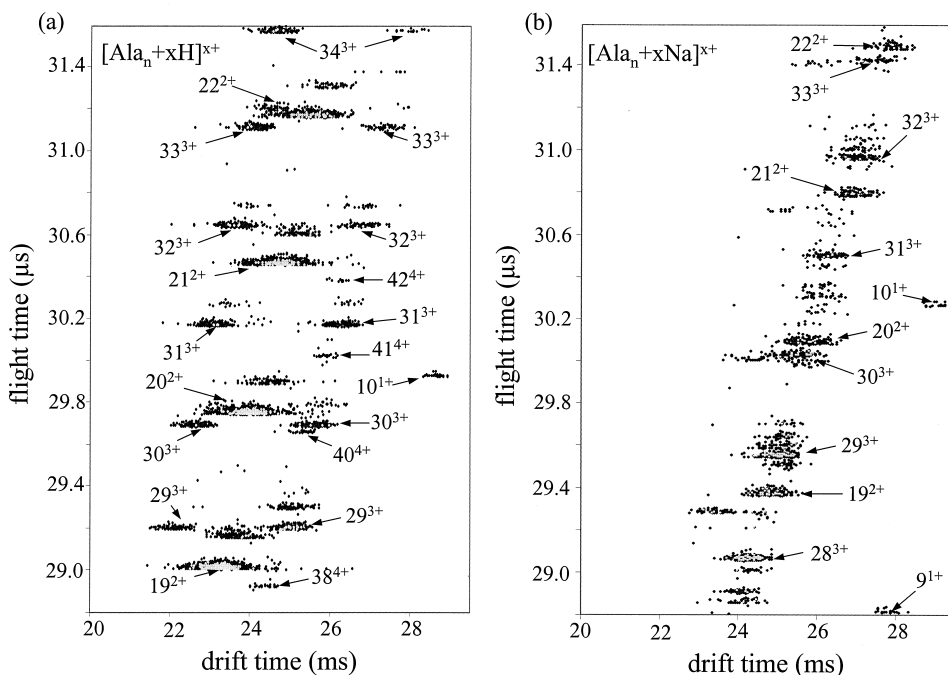


Fig. 3. Two-dimensional plots of a region of nested drift (flight) time data for mixtures of electrosprayed (a) protonated and (b) sodiated polyalanine ions. The electrospray ionization solution conditions used to produce protonated and sodiated peptides are the same as those described in the caption for Fig. 2. The drift time axis for both datasets have been normalized to a pressure of 163.5 Torr and an electric field strength of 137.4 V cm^{-1} . Peaks corresponding to $[\text{Ala}_n + x\text{H}]^{x+}$ (a) and $[\text{Ala}_n + x\text{Na}]^{x+}$ (b) ions are labeled as n^{x+} . Unlabeled features in (b) are much lower intensity than the $[\text{Ala}_n + x\text{Na}]^{x+}$ ions, and correspond to ions having m/z values that are $14/z$ higher than expected $[\text{Ala}_n + x\text{Na}]^{x+}$ species and a high mobility series of $[\text{Ala}_n + \text{Na} + \text{H} + 14]^{2+}$ ions.

conformations upon substitution of two sodium ions for two protons.

It is also worthwhile to consider the shapes of peaks in the drift time distributions; generally, broad features indicate that multiple conformations, which have similar (but not identical) cross sections, are present; or, structural changes occur on the millisecond timescales required for ions to drift through the instrument. Narrow peaks suggest that fewer conformations are present; in particular, experimental peak shapes that are in good agreement with a distribution calculated from the transport equation [31] for a single ion suggest that only a single conformer is present [32]. Peaks in both the sodiated and protonated systems are ~ 3 – 4 times broader than distributions calculated from the transport equation for a single conformation. The $[\text{Ala}_{21} + 2\text{Na}]^{2+}$ distribution also exhibits a tail at lower drift times that

extends to near the drift times observed in the $[\text{Ala}_{21} + 2\text{H}]^{2+}$ distribution. Although the intensity of this tail is small relative to the main feature, it indicates that some more compact states are present. The tailing shape of the peak suggests that the structures of these ions may be changing as ions drift through the instrument.

Comparison of features in Fig. 3 associated with the $[\text{Ala}_n + 3\text{Na}]^{3+}$ and $[\text{Ala}_n + 3\text{H}]^{3+}$ families of ions also reveals large differences in behavior of the sodiated and protonated systems. As discussed previously [23], drift time distributions for $[\text{Ala}_n + 3\text{H}]^{3+}$ ions show two resolved peaks—evidence for at least two stable conformations that do not interconvert over the time scales of these experiments. This can be seen by considering the features at a flight time of $\sim 30.18 \mu\text{s}$; here, $[\text{Ala}_{31} + 3\text{H}]^{3+}$ ions show two resolved peaks along the drift time axis at 21.8 and 25.3 ms.

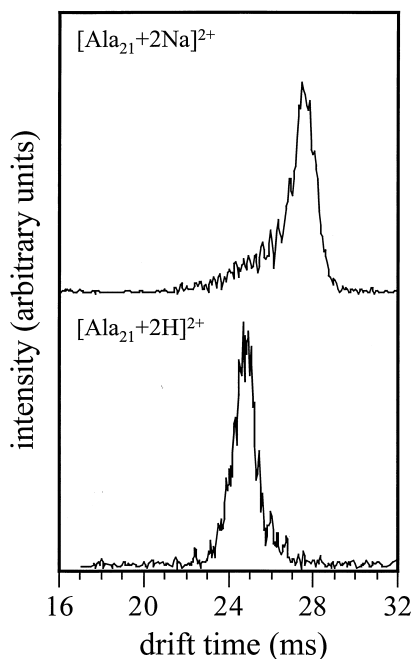


Fig. 4. Drift time distributions for $[\text{Ala}_{21} + 2\text{H}]^{2+}$ and $[\text{Ala}_{21} + 2\text{Na}]^{2+}$ obtained by taking slices through the two-dimensional datasets shown in Fig. 3. The drift time axis for both datasets have been normalized to a pressure of 163.5 Torr and an electric field strength of 137.4 V cm^{-1} . The total intensity of each distribution is shown on an arbitrary normalized scale.

These peaks were previously assigned to hinged helix coil and extended helical motifs, an assignment that is consistent over the range of $[\text{Ala}_n + 3\text{H}]^{3+}$ ions observed.

In sharp contrast, the experimental data for the $[\text{Ala}_n + 3\text{Na}]^{3+}$ ions show only single peaks at each oligomer size. The relatively long drift times of these peaks indicate that these ions have extended conformations. From the plot in Fig. 3, there is no evidence for the folded hinged helix-coil motif for any size of the triply sodiated oligomer.

A more detailed comparison of drift time distributions for the $[\text{Ala}_n + 3\text{H}]^{3+}$ and $[\text{Ala}_n + 3\text{Na}]^{3+}$ ions can be obtained by plotting data for individual oligomer sizes. Fig. 5 shows drift time distributions for triply protonated and sodiated Ala_{27} , Ala_{30} , and Ala_{34} peptides taken from slices through the data at appropriate flight times in Fig. 3. As the length of the $[\text{Ala}_n + 3\text{H}]^{3+}$ polymer chain increases, the higher

mobility ions corresponding to hinged helix-coil states become more abundant than the lower mobility helical states [23]. We have previously rationalized this by noting that longer chains can establish more stabilizing tertiary contacts. Thus, it should become energetically favorable for longer peptides to fold. Additionally, coulomb repulsion decreases with increasing oligomer length, allowing larger oligomers to fold.

Drift time distributions for the triply sodiated $[\text{Ala}_n + 3\text{Na}]^{3+}$ ions show broad peaks with some reproducible but unresolved structural features. For all oligomer sizes, the highest intensity features are observed at longer drift times than observed for the low-mobility extended-helical states (of corresponding $[\text{Ala}_n + 3\text{H}]^{3+}$ ions). The $[\text{Ala}_{27} + 3\text{Na}]^{3+}$ distribution shows a shoulder at 22.7 ms, near the position of the peak observed for the low mobility $[\text{Ala}_{27} + 3\text{H}]^{3+}$ ions. This suggests that extended helical conformations similar to those assigned to the $[\text{Ala}_n + 3\text{H}]^{3+}$ ions may be present in $[\text{Ala}_n + 3\text{Na}]^{3+}$ ions. The $[\text{Ala}_{30} + 3\text{Na}]^{3+}$ and $[\text{Ala}_{34} + 3\text{Na}]^{3+}$ distributions show unresolved tails that extend to lower drift times, indicating that some more compact states are sampled; however, the population of compact states appears to be small. Overall, the data for all sizes show that the total population of ions having drift times that are consistent with folded hinged helix-coil motifs is negligible.

Fig. 6 shows a plot of effective asphericities (Ω_{asp}) determined from Eq. (2) for the main features that are observed in the ion mobility distributions for the $[\text{Ala}_n + 3\text{H}]^{3+}$ and $[\text{Ala}_n + 3\text{Na}]^{3+}$ systems. For comparison we have also shown asphericities that are derived for model α helices (having $\phi = -57^\circ$ and $\psi = -47^\circ$) as well as experimental values for the $[\text{Ala}_n\text{-Lys} + \text{H}]^+$ ions designed by Hudgins et al. [12]. Overall, the asphericities of helical structures increase with increasing oligomer length. Experimental Ω_{asp} values for the most intense features observed for all $[\text{Ala}_n + 3\text{Na}]^{3+}$ sizes fall into a single family. This indicates that the overall shape of different oligomer lengths are similar. The observation that the sodiated data track the protonated data closely, suggests the overall peptide conformations in the two

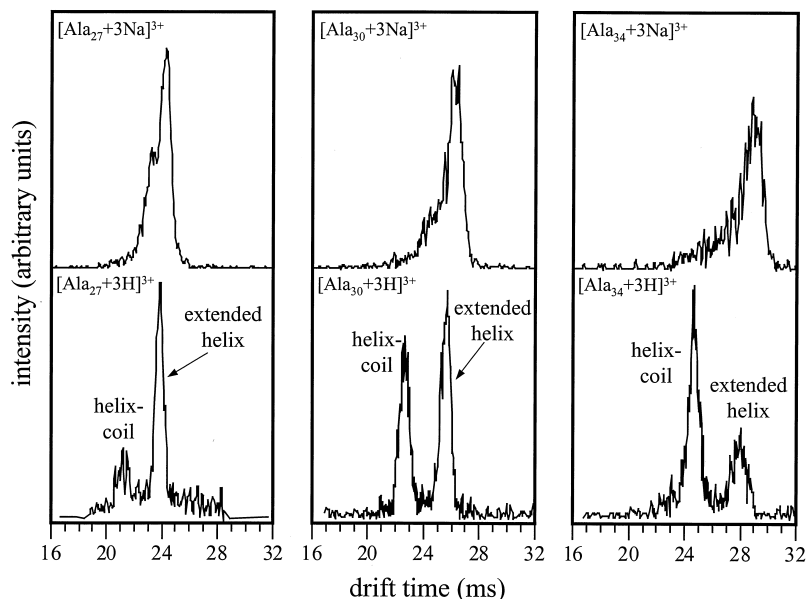


Fig. 5. Drift time distributions for $[\text{Ala}_n + 3\text{H}]^{3+}$ and $[\text{Ala}_n + 3\text{Na}]^{3+}$ ions for $n = 27, 30,$ and 34 . The distributions are obtained by taking slices through the two-dimensional datasets shown in Fig. 3. The drift time axis for both datasets have been normalized to a pressure of 163.5 Torr and an electric field strength of 137.4 V cm^{-1} . The total intensity of each distribution is shown on an arbitrary normalized scale.

systems are related. However, values of Ω_{asp} $[\text{Ala}_n + 3\text{Na}]^{3+}$ are 4%–8% higher than Ω_{asp} values for the low mobility family of largely helical $[\text{Ala}_n + 3\text{H}]^{3+}$ ions [33]. This indicates that the conformations of the $[\text{Ala}_n + 3\text{Na}]^{3+}$ ions are somewhat more extended than the $[\text{Ala}_n + 3\text{H}]^{3+}$ helices.

3.3. Molecular modeling simulations

To obtain additional insight about the conformations of the sodiated peptide ions, as well as structural perturbations that arise upon substitution of sodium ions for protons, we have employed molecular modeling techniques. These calculations are computationally intensive and thus have only been carried out for the $[\text{Ala}_n + 3\text{Na}]^{3+}$ family for the $n = 27, 30,$ and 34 sizes. An issue that arises in these studies is the placement of charge sites. In all cases, we have attached Na^+ at N–H sites along the backbone. To reduce the number of calculations that were necessary we have focused on only those charge-site assignments that gave low-energy conformations that were in good agreement with the asphericities of the

$[\text{Ala}_n + 3\text{H}]^{3+}$ ions. Previously, many charge-site configurations were considered for the $[\text{Ala}_n + 3\text{H}]^{3+}$ ions. These molecular modeling simulations yield distributions of conformations. The conformers that we show below are the lowest energy conformers found for a given charge site assignment, and are representative of many other low-energy geometries. Typical energy differences between the lowest energy conformer and other low energy species are 1–3 kcal mol^{-1} . It should be noted that many additional states have been considered. It is often straightforward to rule out high energy conformations because the calculated asphericities for these geometries are often not consistent with experiment. Although many of these states have been found and considered they are not discussed in detail.

Fig. 7 shows typical low energy conformers for the $[\text{Ala}_{34} + 3\text{H}]^{3+}$ and $[\text{Ala}_{34} + 3\text{Na}]^{3+}$ ions, with protons or Na^+ ions (respectively) placed at the $i = 10, 22,$ and 34 positions. In both cases, calculated Ω_{asp} values are in good agreement with the experimental value (Fig. 6). On average, the $[\text{Ala}_{34} + 3\text{H}]^{3+}$ (10, 22, 34) ion exhibits $\sim 90\%$ $i \rightarrow i + 3$ and $i \rightarrow i +$

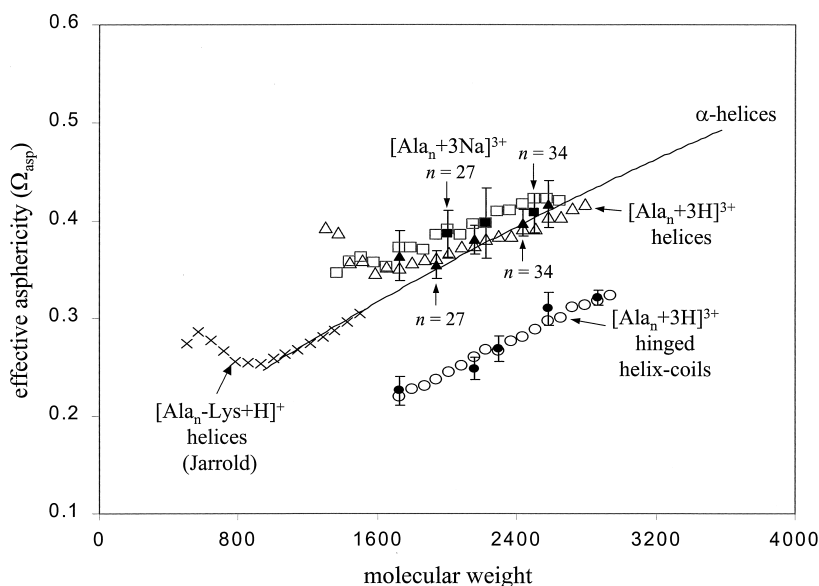


Fig. 6. Effective asphericities for $[\text{Ala}_n + 3\text{H}]^{3+}$ ($n = 18\text{--}38$, open triangles; and $n = 24\text{--}40$, open circles) [23], $[\text{Ala}_n + 3\text{Na}]^{3+}$ ($n = 18\text{--}36$, open squares), and a series of $[\text{Ala}_n\text{--Lys} + \text{H}]^+$ ($n = 5\text{--}19$, represented by crosses), derived from cross sections reported previously by Hudgins et al. [12]. Calculated asphericities for low energy $[\text{Ala}_n + 3\text{H}]^{3+}$ extended helical ($n = 24, 27, 30, 34$, and 36) and hinged helix-coil ($n = 24, 30, 32, 36$, and 40) conformers and $[\text{Ala}_n + 3\text{Na}]^{3+}$ extended helices ($n = 27, 30$, and 34) obtained from molecular dynamics simulations are shown as filled triangles, circles, and squares, respectively. Uncertainties correspond to one standard deviation of the calculated values for the range of stable states found from molecular modeling. The solid line corresponds to calculated values for α -helical Ala_n polymers ($\phi = -57^\circ$ and $\psi = -47^\circ$) containing 10–50 residues.



Fig. 7. Typical low energy conformers obtained from molecular dynamics simulations of $[\text{Ala}_{34} + 3\text{H}]^{3+}$ and $[\text{Ala}_{34} + 3\text{Na}]^{3+}$ with protons or Na^+ ions placed at $i = 10, 22, 34$. Calculated Ω_{asp} values of 0.398 and 0.416 are in good agreement with the experimental values of 0.392 and 0.423 for $[\text{Ala}_{34} + 3\text{H}]^{3+}$ and $[\text{Ala}_{34} + 3\text{Na}]^{3+}$, respectively. Calculated energies for the conformers shown were -150.4 and -264.0 kcal mol $^{-1}$, respectively. Charge sites are shown as close-packed spheres with radii proportional to those of H^+ and Na^+ .

4 helical hydrogen bonding character. Often, slight disruptions in the hydrogen bonding networks are observed near the protonation sites. Substitution of sodium ions for protons at the 10, 22, and 34 positions produces substantially more apparent disruptions in helical character. Only $\sim 70\%$ – 80% of residues in the $[\text{Ala}_{34} + 3\text{Na}]^{3+}$ ($10, 22, 34$) conformer are involved in $i \rightarrow i + 3$ or $i \rightarrow i + 4$ hydrogen bonds. The structure shown in Fig. 7 shows substantial disruptions in helicity for residues that are adjacent to the Na^+ ions placed at $i = 10$ and 22 . In particular, the number of residues associated with the turn increases in order to effectively solvate the larger Na^+ ion. This type of perturbation appears in many of the calculations and appears to be a general difference between protonation and sodiation in helical regions. The effect is somewhat remarkable. By adopting a wider turn the peptide is able to solvate a charge that is aligned with the carbonyl groups on the N-terminal side of the Na^+ site. This has the overall effect of

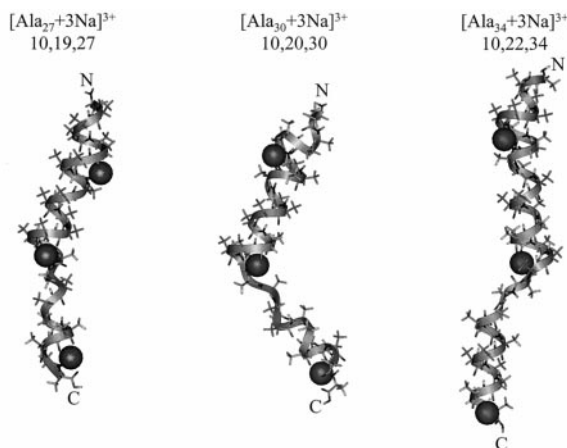


Fig. 8. Representative low energy extended helical conformers obtained for $[\text{Ala}_{27} + 3\text{Na}]^{3+}$ ($i = 10, 19, 27$), $[\text{Ala}_{30} + 3\text{Na}]^{3+}$ ($i = 10, 20, 30$), and $[\text{Ala}_{34} + 3\text{Na}]^{3+}$ ($i = 10, 22, 34$). Calculated Ω_{asp} values are 0.375, 0.396, and 0.416, which agree with the experimental Ω_{asp} values of 0.391, 0.397, and 0.423, respectively. Calculated energies are -221.3 , -248.8 , and -264.0 kcal mol $^{-1}$, respectively.

stabilizing a helical region—similar to the charge capping effect that was found upon incorporating a protonated Lys residue at the C-terminus of polyalanylines [12].

A second type of distortion that is apparent in the sodiated structures is the complete unraveling of several helical turns on the C-terminal side of the charge position; this can be seen at the $[\text{Ala}_{34} + 3\text{Na}]^{3+}$ $i = 22$ position in Fig. 7. Similar results were observed for the $[\text{Ala}_{34} + 3\text{Na}]^{3+}$ ions having $i = 11, 23, 34$ and $11, 25, 34$ charge assignments. The general nature of these types of distortions is shown in Fig. 8 for several low energy conformations of the $[\text{Ala}_{27} + 3\text{Na}]^{3+}$ (10, 19, 27), $[\text{Ala}_{30} + 3\text{Na}]^{3+}$ (10, 20, 30), and $[\text{Ala}_{34} + 3\text{Na}]^{3+}$ (10, 22, 34) ions. All of these structures have calculated asphericities that agree with experiment. For the $[\text{Ala}_{27} + 3\text{Na}]^{3+}$, $[\text{Ala}_{30} + 3\text{Na}]^{3+}$, and $[\text{Ala}_{34} + 3\text{Na}]^{3+}$ conformers, we observe a widening of the helix on the N-terminal side of the $i = 10$ position and an unraveling of the helix around the $i = 19, 20$, or 22 positions (respectively). Simulations of other charge site assignments (e.g. $[\text{Ala}_{30} + 3\text{Na}]^{3+}$ having Na^+ ions assigned to

the 10, 23, 30; 10, 17, 30; and 12, 20, 30 positions) exhibit similar behavior; the locations of helix disruptions for these different charge site assignments vary somewhat, but are generally associated with the positions of the Na^+ ions.

Some insight into factors that influence the unraveling of helical regions can be gained by examining simulations for different oligomer lengths. Small oligomers show more significant disruptions of helicity than larger oligomers (i.e. the helical content observed for the model conformers increases with increasing peptide length). In the conformers shown, the percentage of residues involved in $i \rightarrow i + 3$ or $i \rightarrow i + 4$ hydrogen bonding in the extended helical conformers shown are $\sim 60\%$, 75% , and 80% for $[\text{Ala}_{27} + 3\text{Na}]^{3+}$, $[\text{Ala}_{30} + 3\text{Na}]^{3+}$, and $[\text{Ala}_{34} + 3\text{Na}]^{3+}$, respectively. This trend is observed for other sizes and charge configurations of low energy extended helical conformers that have asphericities in agreement with experimental values. This can be rationalized by noting that coulomb repulsion increases with decreasing size. From the positions of charge sites shown in Fig. 8, we calculate coulomb energies of 57.2, 48.7, and 40.8 kcal mol $^{-1}$ for the $[\text{Ala}_{27} + 3\text{Na}]^{3+}$ (10, 19, 27), $[\text{Ala}_{30} + 3\text{Na}]^{3+}$ (10, 20, 30), and $[\text{Ala}_{34} + 3\text{Na}]^{3+}$ (10, 22, 34) ions [34].

Finally, it is also worth noting that uncertainties associated with the calculated asphericities for the sodiated ions are typically larger than those for their protonated counterparts (Fig. 6). The more substantial loss of hydrogen bonding networks in the sodiated ions results in conformations that are more flexible than their protonated counterparts.

3.4. Where are the hinged helix coils?

Molecular modeling was also used to try to understand the absence of experimental evidence for the hinged helix-coil states for the $[\text{Ala}_n + 3\text{Na}]^{3+}$ ions. Simulations of the protonated ions showed that the position of charge assignments was important in formation of the hinged helix-coil motif [23]. Fig. 9 shows the lowest energy conformations found for two charge site assignments of $[\text{Ala}_{34} + 3\text{H}]^{3+}$ which favor the folded motif: 1, 4, 13 and 1, 5, 10. As

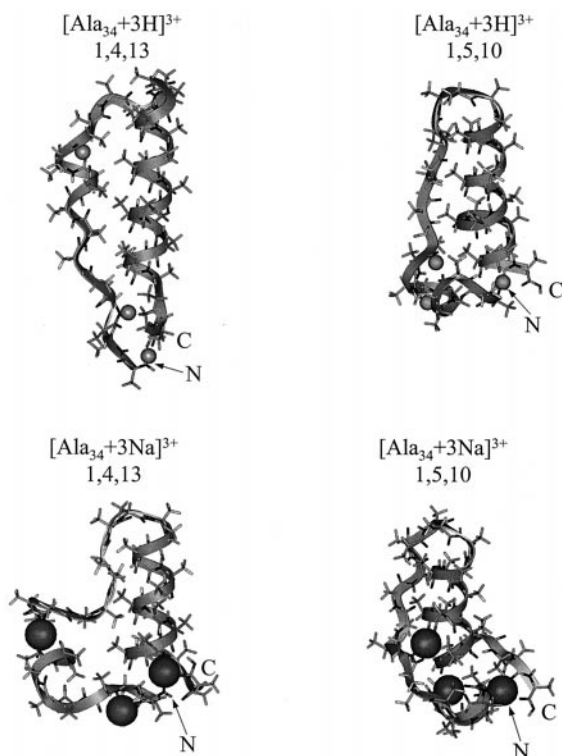


Fig. 9. Typical low energy conformers obtained from molecular dynamics simulations of $[\text{Ala}_{34} + 3\text{H}]^{3+}$ and $[\text{Ala}_{34} + 3\text{Na}]^{3+}$ with protons or Na^+ ions placed at $i = 1, 4, 13$ and $1, 5, 10$. The calculated Ω_{asp} values for the $[\text{Ala}_{34} + 3\text{H}]^{3+}$ 1, 4, 13 and 1, 5, 10 conformers are 0.279 and 0.265, in agreement with the experimental value of 0.281; calculated energies are -118.6 and -101.2 kcal mol^{-1} , respectively. The $[\text{Ala}_{34} + 3\text{Na}]^{3+}$ 1, 4, 13 and 1, 5, 10 conformers have calculated Ω_{asp} values of 0.281 and 0.262; calculated energies are -210.5 and -195.1 kcal mol^{-1} , respectively.

discussed previously [23], placement of three protons on the N-terminal side of the peptide unwinds the initial α -helical structure. The coil-like region that is produced folds back along the helix and interactions of protonated sites with the C-terminal side of the peptide stabilize a substantial C-terminal helical region. Simulations for many different charge site assignments showed that the lowest-energy structures (for an individual charge site assignment) correspond to the hinged helix-coil motifs.

Fig. 9 also shows the lowest energy conformers that are found for simulations of the 1, 4, 13 and 1, 5, 10 charge site assignments of $[\text{Ala}_{34} + 3\text{Na}]^{3+}$. The

results of these simulations also show helical regions of the peptide along the C-terminal side. In fact, these calculations show that folded structures are the most stable states observed for these charge assignments. Although simulations for these charge-site assignments seem to indicate that interactions of the Na^+ ions near the C-terminal side are sufficient to stabilize short helical regions, we note that overall the array of structures found upon sodiation are not as well defined as structures found in simulations of the same charge site positions in the protonated system. Molecular modeling results for other sizes and charge site assignments show similar behavior. As found above for the extended states, substitution of sodium ions for protons appears to increase the flexibility of different conformations. In particular, changes in the interactions that are responsible for solvating the larger sodium ion induce large structural changes in local regions of the oligomer chain.

Some additional insight can be obtained by comparing the relative energetics of folded and extended states for the protonated and sodiated systems. These comparisons are qualitative since the absolute energies depend strongly on the locations of the charge sites. Overall, comparison of the same charge site assignments (extended and folded) for the protonated and sodiated systems shows a larger energy gap between these states in the sodiated system. That is, the extended/folded energy difference is larger in the sodiated system than the protonated system. This qualitative difference suggests that the hinged helix-coil state may not be observed experimentally in the sodiated system because it is less stable than the unfolded state. It seems possible that the larger range of dynamic motion (associated largely with the substantial changes in conformation associated with solvation of the larger sodium) may allow charges to migrate to sites on the C-terminal side of the peptide. The 1, 5, 10, $[\text{Ala}_{34} + 3\text{Na}]^{3+}$ structure shown in Fig. 9 shows a common solvation trend in which the Na^+ intercalates along the helical region found on the C-terminal side of the oligomer. Such a structure might serve as an intermediate for facile charge migration (at least relative to the protonated system).

Finally, it is important to also point out that it is

also possible that the absence of folded states for the $[\text{Ala}_n + 3\text{Na}]^{3+}$ ions arises from differences in the conformer populations that are formed during the electrospray process. Unfolding of polyalanine that are induced by interactions with Na^+ ions in solution prior to ionization would be consistent with the experimental observation of a single peak for the triply sodiated ions. Unfolding transitions in solution at high ionic strengths have been documented extensively for peptides and proteins [35–39].

4. Summary

Ion mobility and molecular modeling techniques have been used to examine the conformations of a series of $[\text{Ala}_n + 3\text{Na}]^{3+}$ ($n = 18\text{--}36$) ions in the gas phase. The results of these studies have been compared to previous studies of $[\text{Ala}_n + 3\text{H}]^{3+}$ ($n = 18\text{--}41$). The previous experimental and theoretical work on the protonated system showed evidence for two conformation types: a series of extended structures that had large helical regions for $n = 18\text{--}39$; and a folded hinged helix-coil geometry, for $n = 24\text{--}41$. The hinged helix-coil geometry becomes the dominant conformation in the protonated system for $n > 32$.

The experimental results for the sodiated system shows that extended structures dominate for all sizes. Unlike the protonated system, there is no strong evidence for a folded hinged helix-coil geometry. Molecular modeling simulations for the $[\text{Ala}_{27} + 3\text{Na}]^{3+}$, $[\text{Ala}_{30} + 3\text{Na}]^{3+}$, and $[\text{Ala}_{34} + 3\text{Na}]^{3+}$ peptides with the three Na^+ ions assigned to an array of possible positions show evidence for extended states that have calculated asphericities that agree with the respective experimental values. As in the protonated systems, good agreement requires that the net position of charge is on the C-terminal side of the peptide (i.e. $\sum i/3 > n/2$) excluding extreme cases when the charges are placed within adjacent turns of a helix. These simulations also show that the extended structures are dominated by large helical regions; however, regions of helix near the sites of Na^+ ion attachment are significantly disrupted by the presence

of the metal. Here, three to five residues may be involved in charge-solvation of the Na^+ ions. In many simulated structures the Na^+ appears to increase the number of residues required for a turn and intercalate into a helical turn; this appears to stabilize regions of helix on the N-terminal side of the charge and destabilize helicity to the C-terminal side.

Simulations of peptides having Na^+ ions distributed along the N-terminal side of the peptide show evidence for folded conformations; in some cases low-energy conformers generated from modeling resemble the hinged helix-coil state observed experimentally for the protonated polyalanines. Overall, the sodiated structures generated from modeling appear distorted and conformations are more flexible than the corresponding protonated systems; solvation of the much larger Na^+ ion disrupts the helical region of the folded state.

One explanation for the absence of strong experimental evidence for the folded hinged helix-coil motif in the sodiated system is that it is less stable relative to the extended helical state (relative to comparisons with identical charge site assignments associated with folded and extended structures in the protonated system). Thus, it appears that differences in stabilities of the different ion states may account for the absence of the folded conformation for the $[\text{Ala}_n + 3\text{Na}]^{3+}$ ions. The absence of folded states for the $[\text{Ala}_n + 3\text{Na}]^{3+}$ ions could also arise from differences in conformers that are produced by electrospray ionization.

Acknowledgements

The authors gratefully acknowledge financial support from the Alfred P. Sloan Foundation, the National Science Foundation (CHE-9625199), and the National Institutes of Health (grant no. 1R01 GM55647-01).

References

- [1] T. Lazaridis, G. Archontis, M. Karplus, *Adv. Protein Chem.* 47 (1995) 231; A.D. Robertson, K.P. Murphy, *Chem. Rev.* 97

- (1997) 1251; S.N. Timasheff, *Adv. Protein Chem.* 51 (1998) 355.
- [2] D. Suckau, Y. Shi, S.C. Beu, M.W. Senko, J.P. Quinn, F.M. Wampler, F.W. McLafferty, *Proc. Natl. Acad. Sci. USA* 90 (1993) 790; T.D. Wood, R.A. Chorush, F.M. Wampler, D.P. Little, P.B. O'Connor, F.W. McLafferty, *ibid.* 92 (1995) 2451.
- [3] D.S. Gross, P.D. Schnier, S.E. Rodriguez-Cruz, C.K. Fagerquist, E.R. Williams, *Proc. Natl. Acad. Sci. USA* 93 (1996) 3143; P.D. Schnier, W.D. Price, R.A. Jockusch, *J. Am. Chem. Soc.* 118 (1996) 7178.
- [4] X. Zhang, C.J. Cassidy, *J. Am. Soc. Mass Spectrom.* 7 (1996) 1211.
- [5] I.A. Kaltashov, C. Fenselau, *Proteins: Struct., Funct., Genet.* 27 (1997) 165.
- [6] T. Wyttenbach, J.E. Bushnell, M.T. Bowers, *J. Am. Chem. Soc.* 120 (1998) 5098.
- [7] D.E. Clemmer, R.R. Hudgins, M.F. Jarrold, *J. Am. Chem. Soc.* 117 (1995) 10141; K.B. Shelimov, D.E. Clemmer, R.R. Hudgins, M.F. Jarrold, *J. Am. Chem. Soc.* 119 (1997) 2240; K.B. Shelimov, M.F. Jarrold, *J. Am. Chem. Soc.* 119 (1997) 2987; R.R. Hudgins, J. Woenckhaus, M.F. Jarrold, *Int. J. Mass Spectrom. Ion Processes* 165/166 (1997) 497; J.L. Fye, J. Woenckhaus, M.F. Jarrold, *J. Am. Chem. Soc.* 120 (1998) 1327.
- [8] S.J. Valentine, J.G. Anderson, A.D. Ellington, D.E. Clemmer, *J. Phys. Chem. B* 101 (1997) 3891; S.J. Valentine, A.E. Counterman, D.E. Clemmer, *J. Am. Soc. Mass Spectrom.* 8 (1997) 954.
- [9] C.T. Reimann, P.A. Sullivan, J. Axelsson, A.P. Quist, S. Altmann, P. Roepstorff, I. Velazquez, O. Tapia, *J. Am. Chem. Soc.* 120 (1998) 7608.
- [10] P.G. Wolynes, *Proc. Natl. Acad. Sci. USA* 92 (1995) 2426.
- [11] T. Wyttenbach, G. von Helden, M.T. Bowers, *J. Am. Chem. Soc.* 118 (1996) 8355.
- [12] R.R. Hudgins, M.A. Ratner, M.F. Jarrold, *J. Am. Chem. Soc.* 120 (1998) 12974.
- [13] R.R. Hudgins, Y. Mao, M.A. Ratner, M.F. Jarrold, *Biophysical J.* 76 (1999) 1591.
- [14] R.R. Hudgins, M.F. Jarrold, *J. Am. Chem. Soc.* 121 (1999) 3494.
- [15] S.J. Valentine, A.E. Counterman, C.S. Hoaglund-Hyzer, D.E. Clemmer, *J. Phys. Chem. B* 8 (1999) 1203; S.J. Valentine, A.E. Counterman, D.E. Clemmer, *J. Am. Soc. Mass Spectrom.* 10 (1999) 1188.
- [16] S.C. Henderson, J. Li, A.E. Counterman, D.E. Clemmer, *J. Phys. Chem. B* 103 (1999) 8780.
- [17] R. Orlando, C.A. Bush, C. Fenselau, *Biomed. Env. Mass Spectrom.* 19 (1990) 747; S. Lee, T. Wyttenbach, M.T. Bowers, *Int. J. Mass Spectrom. Ion Processes* 167 (1997) 605; Y. Liu, D.E. Clemmer, *Anal. Chem.* 69 (1997) 2504; S.P. Gaucher, J.A. Leary, *ibid.* 70 (1998) 3009; M.T. Cancelli, S.G. Penn, C.B. Lebrilla, *ibid.* 70 (1998) 663; K. Tseng, J.L. Hedrick, C.B. Lebrilla, *ibid.* 71 (1999) 3747; H. Desaire, J.A. Leary, *ibid.* 71 (1999) 1997.
- [18] C.S. Hoaglund, Y. Liu, A.D. Ellington, M. Pagel, D.E. Clemmer, *J. Am. Chem. Soc.* 119 (1997) 9051; M.A. Freitas, S.D. Shi, C.L. Hendrickson, A.G. Marshall, *ibid.* 120 (1998) 10187; J.M. Robinson, M.J. Greig, R.H. Griffey, V. Mohan, D.A. Laude, *Anal. Chem.* 70 (1998) 3566; R.H. Griffey, M.J. Greig, J.M. Robinson, D.A. Laude, *Rapid Comm. Mass Spectrom.* 13 (1999) 113; E.F. Strittmatter, P.D. Schnier, J.S. Klassen, E.R. Williams, *J. Am. Soc. Mass Spectrom.* 10 (1999) 1095.
- [19] S. Samuelson, G.J. Martyna, *J. Phys. Chem. B* 103 (1999) 1752.
- [20] X. Cheng, C. Fenselau, *J. Am. Chem. Soc.* 115 (1993) 10327; M.A. Freitas, C.L. Hendrickson, M.R. Emmett, A.G. Marshall, *J. Am. Soc. Mass Spectrom.* 9 (1998) 1012; D.J. Butcher, K.G. Assano, D.E. Goeringer, S.A. McLuckey, *J. Phys. Chem. A* 103 (1999) 8664.
- [21] P.Y. Chou, G.D. Fasman, *Biochem.* 13 (1974) 211; K.T. O'Neil, W.F. DeGrado, *Science* 250 (1990) 646; P.C. Lyu, M.I. Liff, L.A. Marky, N.R. Kallenbach, *ibid.* 250 (1990) 669; G.L. Millhauser, C.J. Stenland, P. Hanson, K.A. Bolin, F.J.M. van de Ven, *J. Mol. Biol.* 267 (1997) 963; E.J. Spek, C.A. Olson, Z. Shi, N.R. Kallenbach, *J. Am. Chem. Soc.* 121 (1999) 5571.
- [22] R.R. Hudgins, M.F. Jarrold, *J. Phys. Chem. B* 104 (2000) 2154.
- [23] A.E. Counterman, D.E. Clemmer, *J. Am. Chem. Soc.*, submitted.
- [24] At this point the hinged helix-coil motif is the lowest energy folded state for a given charge site assignment that is found in any simulations that we have done. We note that the total energy of the folded state is higher than that for extended helices (obtained for other $\Sigma i/3 > n/2$ assignments). We are still investigating the origin of these energy differences.
- [25] Ion mobility spectrometry methods are discussed in the following references: D.F. Hagen, *Anal. Chem.* 51 (1979) 870; J.C. Tou, G.U. Boggs, *ibid.* 48 (1976) 1351; Z. Karpas, M.J. Cohen, R.M. Stimac, R.F. Wernlund, *Int. J. Mass Spectrom. Ion Processes* 83 (1986) 163; R.H. St. Louis, H.H. Hill, *Crit. Rev. Anal. Chem.* 21 (1990) 321; G. von Helden, M.T. Hsu, P.R. Kemper, M.T. Bowers, *J. Chem. Phys.* 95 (1991) 3835; M.F. Jarrold, *J. Phys. Chem.* 99 (1995) 11.
- [26] For recent reviews of ion mobility studies of biomolecules see: D.E. Clemmer, M.F. Jarrold, *J. Mass Spectrom.* 32 (1997) 577; Y. Liu, S.J. Valentine, A.E. Counterman, C.S. Hoaglund, D.E. Clemmer, *Anal. Chem.* 69 (1997) 728A; M.F. Jarrold, *Acc. Chem. Res.* 32 (1999) 360; C.S. Hoaglund-Hyzer, A.E. Counterman, D.E. Clemmer, *Chem. Rev.* 99 (1999) 3037.
- [27] C.S. Hoaglund, S.J. Valentine, C.R. Sporleder, J.P. Reilly, D.E. Clemmer, *Anal. Chem.* 70 (1998) 2236; S.C. Henderson, S.J. Valentine, A.E. Counterman, D.E. Clemmer, *ibid.* 71 (1999) 291.
- [28] C.A. Srebalus, J. Li, W.S. Marshall, D.E. Clemmer, *Anal. Chem.* 71 (1999) 3918.
- [29] *InsightII*; BIOSYM/MSI, San Diego, CA, 1995.
- [30] A.A. Shvartsburg, M.F. Jarrold, *Chem. Phys. Lett.* 261 (1996) 86.
- [31] E.A. Mason, E.W. McDaniel, *Transport Properties of Ions in Gases*, Wiley, New York, 1988.
- [32] G. von Helden, M.T. Hsu, N. Gotts, M.T. Bowers, *J. Phys. Chem.* 97 (1993) 8182; M.F. Jarrold, J.E. Bower, *J. Chem. Phys.* 98 (1993) 2399.
- [33] This comparison is made for only those oligomers with $n >$

22. For smaller sizes asphericities for the protonated peptides increase slightly with decreasing size, whereas those for the sodiated system decrease with decreasing size. We speculate that the increase in asphericities for small protonated peptides corresponds to an unraveling of the helix—induced by the relatively high coulomb energy on these smaller oligomers.
- [34] Coulomb energies were calculated from $CE = \sum_{i=1}^n \sum_{j=i+1}^{n-1} [q_i q_j / (4\pi\epsilon_0)\epsilon_r r_{i,j}]$, where q_i and q_j are the magnitude of charge at positions i and j , respectively; ϵ_0 is the permittivity of free space, ϵ_r is the dielectric constant (taken to be 1.0), and $r_{i,j}$ is the distance between charges.
- [35] T. Arakawa, S.N. Timasheff, *Biochemistry* 23 (1984) 5912.
- [36] S. Marqusee, R.L. Baldwin, *Proc. Natl. Acad. Sci. USA* 84 (1987) 8898.
- [37] T. Arakawa, S.N. Timasheff, *Biochemistry* 29 (1990) 1924.
- [38] J.M. Scholtz, E.J. York, J.M. Stewart, R.L. Baldwin, *J. Am. Chem. Soc.* 113 (1991) 5102.
- [39] J.S. Smith, J.M. Scholtz, *Biochemistry* 35 (1996) 7292.